

Experimental evaluation of the temperature related behaviour of pigment based coloured BIPV modules integrated in a ventilated façade

Martina Pelle^{*}, Martino Gubert, Enrico Dalla Maria, Alexander Astigarraga, Stefano Avesani, Laura Maturi

Eurac Research, Institute for Renewable Energies, Bolzano, Italy

ARTICLE INFO

Keywords:

Coloured BIPV
Ventilated façade
Ross coefficient

ABSTRACT

Coloured BIPV installations require an accurate balance between aesthetic and energy aspects. This study explores the integration of Building Integrated Photovoltaic (BIPV) modules into building envelopes to enhance energy efficiency while maintaining aesthetic appeal. To achieve this goal, a real-scale mock-up was realized within the INFINITE project at the PV Integration Lab of Eurac Research to investigate the influence of aesthetic features (mainly given by different colors) on the energy performance of BIPV modules. Supported by an extensive monitoring campaign, this work delves into the performance of BIPV modules of five colors and finishes in both indoor and real exposure conditions. These modules serve as the outer layer of a prefabricated rain screen facade for building retrofitting. The study highlights that darker colors exhibit higher efficiency under standard test conditions but are also correlated with higher operating temperatures. Consequently, the differences in energy efficiency among the colors, observed during indoor tests, are significantly reduced when analyzing the energy produced under real exposure conditions. This observation underscores the intricate balance between maximizing energy generation and mitigating thermal stress on BIPV modules, while preserving aesthetic features. By providing empirical evidence of color-specific performance characteristics, this work offers insightful results for colored BIPV research and customized product optimization.

1. Introduction

The climate neutrality targets set by the European Parliament are becoming increasingly ambitious and rapidly approaching. The goal outlined in the “Green Deal” is to achieve a substantial reduction in climate-altering emissions (measured in tons of CO₂ equivalent) by 2030, with the aim of reaching climate neutrality – also known as “Zero Carbon” – by 2050. One of the key actions in this perspective is the renovation of buildings, which are responsible for over 36 % of emissions and 40 % of energy consumption. Transforming the building stock into nearly zero or positive energy is crucial for meeting global decarbonization targets [1]. To do so, deep retrofit actions are needed for reducing the primary energy consumption of over 60 %. The European directive on the minimum energy performance of buildings (EPBD) [2], sets out the requirement for residential buildings to improve their energy performance through deep retrofit, to achieve at least an energy performance class E by 2030.

In this respect, the use of envelope solutions devoted to deep retrofit

based on the concepts of prefabrication and process industrialization, seems to have the highest potential for improving the efficiency, the quality and sustainability of the proposed solutions, while guaranteeing multifunctionality and replicability. On the other hand, on site energy production is crucial for minimizing the buildings’ net energy consumption. Therefore, the integration of energy production strategies in the building envelope is crucial to unlock the energy generation potential of façade. In the last years Building Integrated Photovoltaic (BIPV) technologies have emerged as a promising solution to harvest solar energy on-site, facilitating the shift from fossil fuels to cleaner energy sources [3]. BIPV systems are multifunctional envelope elements that seamlessly integrate into the building skin, offering aesthetic, technological, and energy benefits [4]. Nevertheless, designing BIPV envelope solutions poses a significant challenge in balancing aesthetic and energy aspects, since achieving an optimal technical performance while meeting the architectural requirements of the built environment is essential [5,6].

Within the INFINITE project, a real-scale mock-up has been

^{*} Corresponding author.

E-mail address: martina.pelle@eurac.edu (M. Pelle).

<https://doi.org/10.1016/j.enbuild.2024.114763>

Received 31 March 2024; Received in revised form 23 August 2024; Accepted 4 September 2024

Available online 7 September 2024

0378-7788/© 2024 The Authors. Published by Elsevier B.V. This is an open access article under the CC BY license (<http://creativecommons.org/licenses/by/4.0/>).

implemented at the PV Integration Lab of Eurac Research to examine the impact of aesthetic features on the energy performance of coloured BIPV modules. This study is supported by an extensive monitoring campaign that delves into the performance of BIPV modules with various colours and finishing in real exposure conditions. The modules are integrated as the outer layer of a prefabricated rain screen façade system designed for building retrofitting purposes.

The integration of indoor testing and outdoor monitoring data in this research allows for a comprehensive understanding of the interplay between aesthetic aspects and energy performance in coloured BIPV installations. By exploring the impact of different colours and finishing options on the energy efficiency of the integrated façade, this study contributes to the development of guidelines for designing and optimizing such systems. The findings will enable architects, engineers, and building professionals to make informed decisions when incorporating coloured BIPV modules into building envelopes, ensuring a balanced

approach that maximizes both aesthetic appeal and energy generation.

2. Methodology

The methodology employed for assessing the aesthetic impact on the energy performance considering diverse coloured Building Integrated Photovoltaic (BIPV) modules is grounded in an experimental investigation encompassing both controlled indoor testing (under Standard Test Conditions, STC) and extensive outdoor monitoring, with the BIPV modules operating in real operating conditions over three months, from April to June 2023. This dual approach facilitates the evaluation of colour-specific characteristics under standardized conditions, while concurrently elucidating additional mechanisms influencing energy performance appearing when operating in real environments characterized by elevated temperatures and variable irradiation levels.



Fig. 1. Final layout of the Flexilab mock-up with the different multifunctional prefabricated façade cladding (i) BIPV, (ii) BIST (building integrated solar thermal) in black, and (iii) GREEN (bottom right). (For interpretation of the references to color in this figure legend, the reader is referred to the web version of this article.)

2.1. Mock-up description

A 16 m² full-scale functional and performance mock-up of an industrialized prefab wooden-based multifunctional façade has been realized within the INFINITE project. The overall aim of the mock-up was to demonstrate the technological development of 3 different multifunctional prefabricated façade cladding as reported in (Fig. 1): (i) BIPV, (ii) BIST (building integrated solar thermal) and (iii) GREEN (vertical green wall modules as cladding) looking at the installation phases and monitoring the performance. The main design concept was to define as much configuration as possible for each technology such as orientation, dimensions, finishing, fixation system, interaction between different claddings. The mock-up is composed by 2 main parts: (i) the prefabricated wood-based façade that embeds the insulation layer, (ii) the 3 different cladding solutions. This paper focuses on the BIPV kit (Fig. 1) while the other two cladding typologies (BIST and GREEN) are given for the sake of completeness. The fixation system is composed by a set of glued aluminium brackets on the back of the PV module to be “hanged” into horizontal aluminium profile fixed mechanically on the prefab façade. The interface between these horizontal profiles was made by 60 mm vertical wood mullion every 600 mm to allow the ventilation on the back of the modules.

Fig. 2 shows the results of the final design of BIPV kit mock-up, which has been conceived to increase as much as possible the prefabrication phase and minimize the onsite activities. For these reasons the horizontal aluminum profiles were installed in the factory during the manufacturing of the wooden structure, while the installation of BIPV panels was performed on site as the last construction phase, to minimize the risks of damages on the glass-glass modules. After the installation of the prefabricated modules due to the high level of PV panels damage risk. A further aspect that was taken into consideration was the weather protection of supporting structure (vertical wood mullion) via the application of a waterproof membrane as shown in Fig. 3. The onsite installation phase, including the installation of the BIPV panels and their electrical connection, lasted 45 min with an average of 5:40 min/m² (Fig. 1).

Focusing on the BIPV cladding, to evaluate the influence of different colours and glass structures on the BIPV electric performance, the modules' layout on the mock-up has been designed to host 5 different coloured and textured BIPV modules. Furthermore, the mock-up hosts 3 standard sizes of the BIPV kit plus some custom sizes (for the bottom row) (Fig. 4). The number and typology of the modules installed in the mock-up are summarized in Table 1. The colouring technology for all the colours consists of coloured glass panes coated with absorptive ceramic dyes. The ceramic coating is prepared and then fixed on the glass surface

via a thermomechanical process. The ceramic dyes that form the colour coating are uniformly distributed in the layer and reproduce a single colour. The coloured glasses have been laminated in glass-glass modules, where the back glasses are coated with a blackish colour to provide a uniform appearance of the background, blending with the cells. For the same reason, specific black tape has been used to conceal the fingers and busbars. The cells in each module are standard monocrystalline PERC cells, connected in series.

2.2. Design of the outdoor experiment on the Flexi mock-up

To assess properly the performance of the PV modules in real outdoor condition, a series of sensors have been installed on the mock-up. The modules of each colour are wired to a dedicated microinverter that allow the operation at M_{PPT} . Concerning the electrical scheme, all the modules of the same colour have been connected in series. The operation conditions of the selected microinverters have been previously tested indoor with a photovoltaic string simulator (Ametek ETS600X8D). This verification takes the input of the I-V parameters provided by the solar simulator and recreates different operating conditions of the PV string. Therefore, the optimal matching of micro inverters and PV strings was done using the results of the mentioned verification. This connection configuration allows to monitor separately the electric behaviour of the modules with the same colour, by means of dedicated transducer that provides DC current and voltage readings. In addition, a total of 43 temperature sensors have been installed on the back of the PV modules, and 12 temperature sensors on the wooden structure, to evaluate the evolution of the temperatures in the ventilated cavity. For the same reason, a set of 6 anemometers are installed in the cavity. A pyranometer is installed on the same modules' plan, to measure the global irradiance impinging on the modules' plan, and a meteo-station present in the outdoor laboratory will provide the required ambient parameters. The detail of the monitored parameters is provided in Table 2. The position of the temperature sensors (PT100) on the modules' back surface is provided in Fig. 5. The detail of the position temperature sensors (PT100) on the modules' back surface, for each module's typology, is provided in Fig. 6.

2.3. Monitoring and data acquisition system architecture design

The outdoor experimental facility Flexilab is equipped with a monitoring system that performs the acquisition of the sensors located on the mock-up structure and deals with the transmissions and storage of acquired data on the Eurac ICT infrastructure. The schematization of the data acquisition system architecture is provided in Fig. 7.

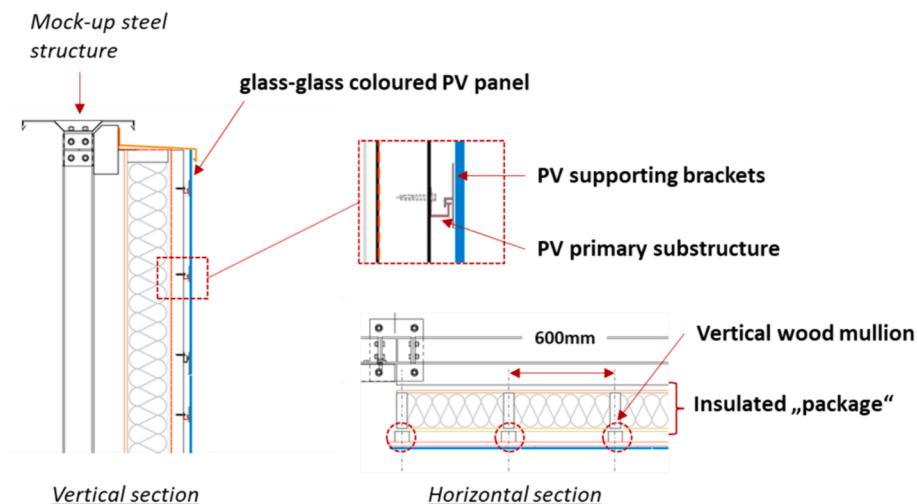


Fig. 2. Vertical and horizontal section of the BIPV mock-up.

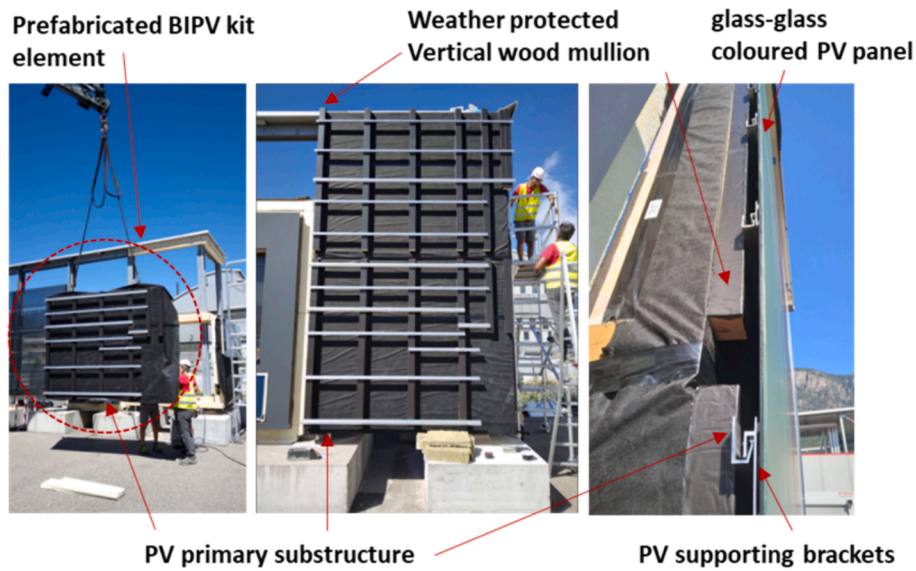


Fig. 3. Installation of the prefabricated BIPV modules on the primary fixation system.

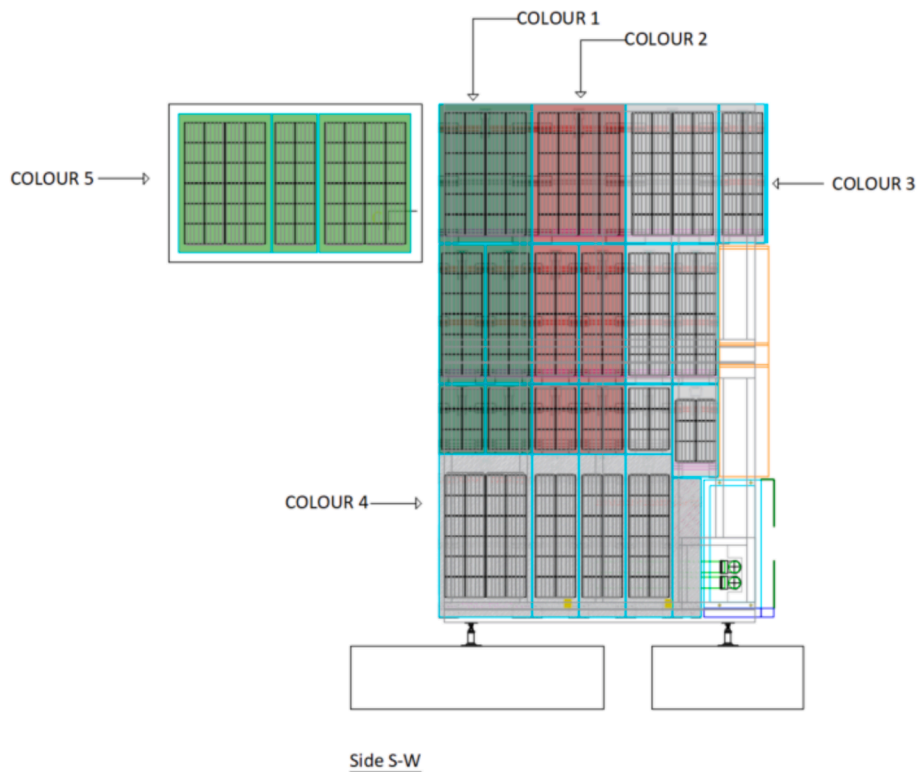


Fig. 4. Layout of the BIPV modules on the Flexilab façade mock-up.

The core of the system is hosted in a thermal box to ensure proper climatic conditions for the operation of the more critical electronic component. All transducers are wired from the facade to this technical room where a benchtop measure unit (multiplexed digital multimeter DMM, model Keysight 34980A) performs the actual acquisition of the voltage/current transduced measurands to digital. This device takes the measurement every 30 s, acquiring sequentially each transducer [Table 2](#).

An industrial PC controls the operation of the DMM and performs the actual delivery of the acquired data to the data-storage solution, a database (InfluxDB) hosted on the Eurac ICT infrastructure.

Historical system data can be accessed through database queries. Tools such as Chronograf and Grafana simplify this operation by allowing quick setting of query parameters and facilitating data navigation and graph and dashboard creation. Lastly, Researchers can carry out further detailed analysis of the monitored installation performances by downloading the raw data of the entire monitoring period from the database.

Table 1

Detail of the number of modules installed in the Flexilab mock-up, broken per colour and typology. The nominal string power refers to the cumulative power of the string for each colour in the mock-up.

| Colour number | Colour (ceramic coating) | Front glass typology | Module's typology | Number of pieces | Nominal string power [W] |
|---------------|--------------------------|----------------------|-------------------------------|------------------|--------------------------|
| 1 | Forest green | Satin | 24 cells | 1 | 223.78 |
| | | | 12 cells | 2 | |
| | | | 6 cells | 2 | |
| 2 | Mahogany brown | Satin | 24 cells | 1 | 229.43 |
| | | | 12 cells | 2 | |
| | | | 6 cells | 2 | |
| 3 | Signal white | Satin | 24 cells | 1 | 194.32 |
| | | | 12 cells | 3 | |
| | | | 6 cells | 1 | |
| | | | 6 cells, custom | 1 | |
| | | | 360x730 mm Dummy, 360x1100 mm | 1 | |
| 4 | Signal white | Structured | Dummy, 224x1100 mm | 1 | 143.74 |
| | | | 24 cells, custom | 1 | |
| | | | 730x1285 mm | 3 | |
| 5 | Copper green | Satin | 24 cells | 2 | 196.37 |
| | | | 12 cells | 1 | |

3. Experimental assessment for energy integration

3.1. Indoor test results

Before the installation on the mock-up, the modules have undergone indoor testing to check their quality and electric performance at standard conditions (Fig. 8). The indoor characterization of BIPV modules has been performed by means of a solar simulator and an

Table 2

Detail of the monitored parameters and installed sensors in the Flexi mock-up for the BIPV kit outdoor monitoring.

| ID | Name | Description | Source (sensor, computation) | Unit | Acquisition frequency | Location | Number of sensors |
|-------------------|-------------------------------|--|------------------------------|------------------|-----------------------|--|-------------------|
| T _{mn} | Temp. Back module | Module temperature measured on the backsheet | PT 100 | °C | 30 s | module back surface | 43 |
| T _{bs} | Temp. Wooden surface | Temperature of the rubner module surface | PT 100 | °C | 30 s | module back surface | 12 |
| P _{mpp} | Inverter Input power | MPPT total input power DC | Microinverter | W | 30 s | microinverter | 5 |
| I _{mpp} | MPP current | Maximum power point current | Current/Voltage transducer | A | 30 s | microinverter | |
| V _{mpp} | MPP voltage | Maximum power point voltage | | V | 30 s | microinverter | |
| I _m | Global irradiance | Global irradiance on the modules plane | Pyranometer | W/m ² | 30 s | On the modules' plan | 1 |
| V _{ag} | Air speed | Air speed between PV module and substructure | Anemometer | m/s | 30 s | Air gap between PV module and substructure | 6 |
| θ _w | Wind direction | Wind direction | Anemometer | deg | 30 s | external | 1 |
| V _w | Wind speed | Wind speed | Anemometer | m/s | 30 s | external | 1 |
| T _{amb} | Ambient Temperature | External ambient Temperature | Temperature sensor | °C | 30 s | external | 1 |
| RH _{amb} | Relative humidity | External relative humidity | Humidity sensor | % | 30 s | external | 1 |
| I _d | Diffuse horizontal irradiance | Diffuse horizontal irradiance | Pyranometer | W/m ² | 30 s | external | 1 |
| I _g | Global horizontal irradiance | Global horizontal irradiance | Pyranometer | W/m ² | 30 s | external | 1 |
| I _b | Direct normal irradiance | Direct normal irradiance on a horizontal plane | Pyrheliometer | W/m ² | 30 s | external | 1 |
| θ _s | Azimuth | Solar azimuth | Pyranometer | deg | 30 s | external | 1 |

electroluminescence (EL) camera provided by indoor “Solare PV Lab” of Eurac Research.

The pulsed light solar simulator is in class “AAA”, according to the international standard IEC 60904–9. It measures the electrical performance of PV modules, allowing the performance analysis of a PV cell or the comparison among different technologies in controlled conditions. It measures the PV module’s IV curve under standard conditions. The measurements detect the energy performance of the module in different combinations of irradiance (0–1000 W/m²), in accordance with UNI CEI EN ISO/IEC 17025:2005. The test accredited is the Performance at STC (MQT 06.1) for PV modules according to the standard IEC 61215:2021. The simulator set up has been adjusted to host modules of different sizes and colours (Fig. 9). The electroluminescence camera is a VIS-SWIR InGaAs camera with a quantum efficiency over 60 % at 1–1.2 μm and sensor of 640x512 pixels. This camera enables the implementation of the test following IEC TS 60904-13:2018 indications. It shows the path taken by the electrons along the circuitry in the module and focuses on the effect of the non-transparent glass in the EL signal emission. The results of electroluminescence at normal incidence demonstrate a good reception of the signal in the colored modules compared to transparent glass technology (Fig. 10).

The electrical performance of PV modules has been measured at standard conditions by means of I-V multi-flash test (60904-1:2021), to measure the main electrical parameters characterizing each module to be installed in the Flexilab mock-up. The test allows to define the characteristic current–voltage curve (IV curve) and voltage–power curve, as well as the shunt and series resistances, the current and voltage at maximum power point, the fill factor. Starting from this information, it is possible to calculate the efficiency of the modules. This parameter is usually calculated considering the total surface of each module A, its maximum power production P_{max} and a standard amount of irradiation impinging on the module’s surface I (1000 W/m²) (EQ. 1).

$$\eta = \frac{P_{max}}{I \cdot A} \cdot 100 [\%] \tag{1}$$

In the following we provide calculation of the maximum efficiency as a function of the sole colour, neglecting the ratio between active area and passive area, which is a specific feature of each module’s size. Therefore, we considered for each module only its active area, i.e., the area interested by the solar cells. In this way we can compare the efficiency of the modules of the same colour and compare the effect of the

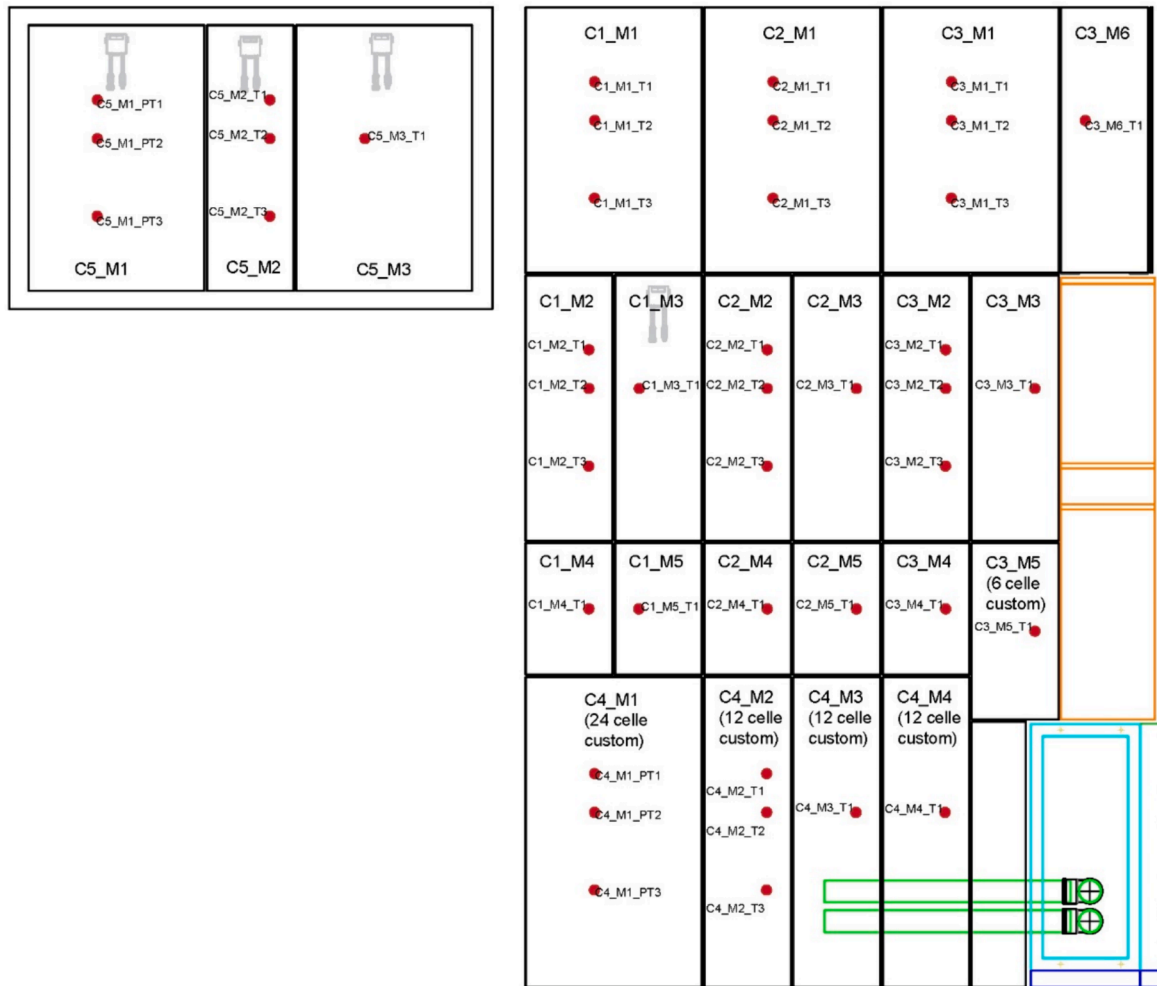


Fig. 5. Temperature sensors (PT100, red dots) position on the modules' back surfaces. (For interpretation of the references to color in this figure legend, the reader is referred to the web version of this article.)

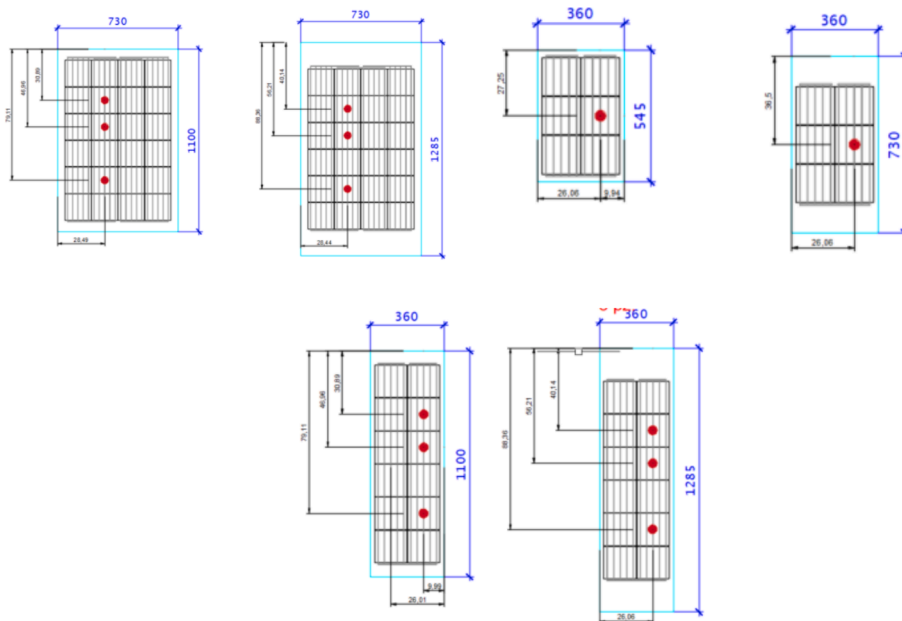


Fig. 6. Temperature sensors (PT100) position on the modules' back surface. Detail of the position for each module's typology: top row from the left: 24 cells modules, standard size and custom size; 6 cells modules, standard size and custom size; 12 cells modules, standard size and custom size.

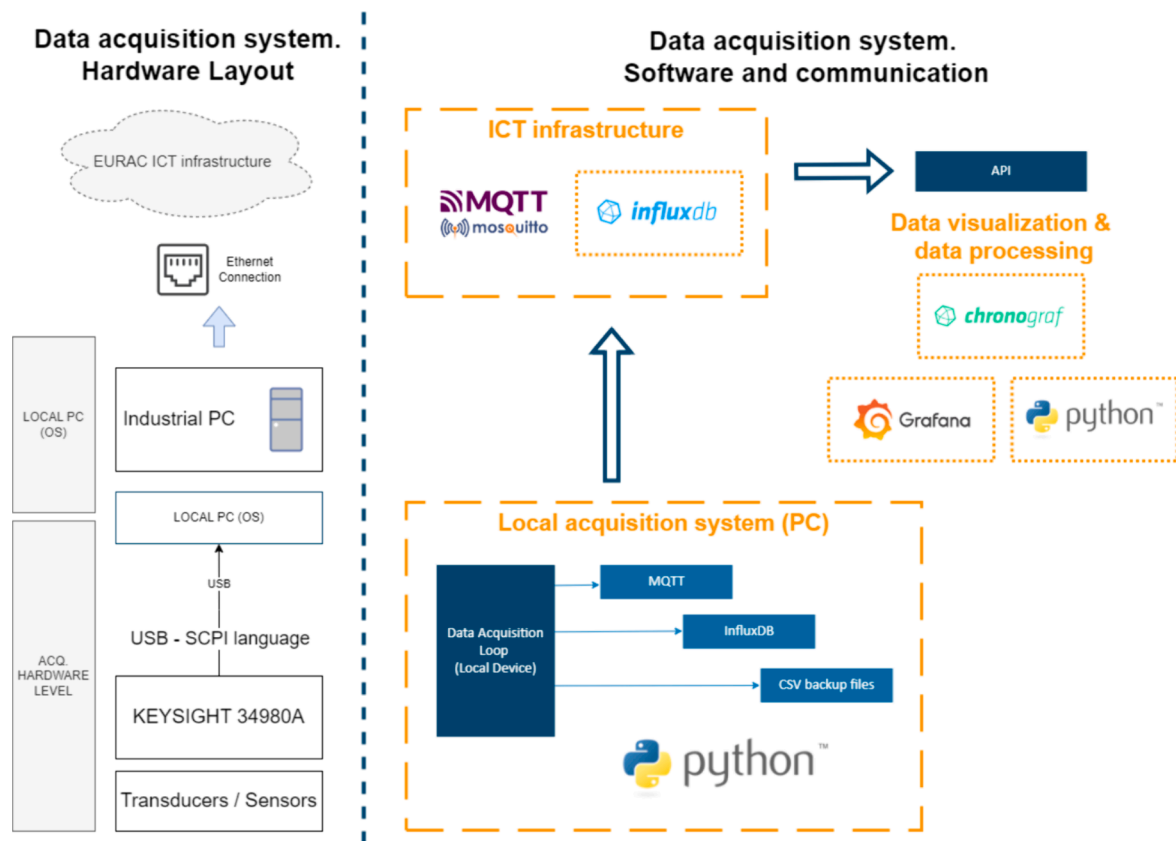


Fig. 7. Scheme of the data acquisition and communication system architecture.



Fig. 8. Modules tested in the indoor “Solare PV Lab” of Eurac Research.



Fig. 9. The simulator set adjusted to host modules of different sizes and colours. From the left: six cells module, 12 cells module, 24 cells module.

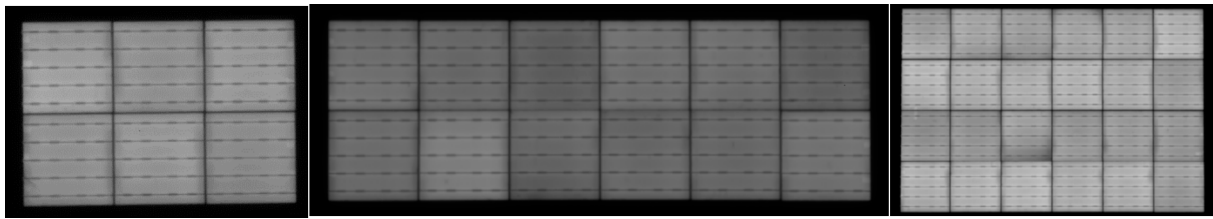


Fig. 10. Example of the electroluminescence test results, example. From the left: six cells module, 12 cells module, 24 cells module.

coloured layers on the module’s efficiency. The average efficiencies, broken by colour, are reported in Fig. 11. The efficiencies of the INFINITE Flexilab colours are compared to a reference transparent module of the same typology, provided by the same manufacturer. The results shows that brightest colours (white and copper green) provide the lowest efficiency, while darker colours (mahogany and forest green) perform better. This is due to the highest reflection in the visible range of the solar spectrum needed to render bright colours. The results of the indoor tests show, as expected, a minimum effect of the colour on the open circuit voltage and the fill factor (Table 3 and Fig. 12), while the colour affects more the short circuit current, which is proportional to the amount of irradiation reaching the cells surface, and as a consequence, the maximum power production (Fig. 13).

3.2. Outdoor monitoring

The data acquired with a time resolution of 30 s via the installed sensors have been analysed to provide insight on the module operating behaviour. The electric parameters provided for each colour string by the inverter, are used to analyse the energy yield of each colour set. Furthermore, the extensive temperature mapping of the façade solution has been conceived to enable the analysis of the temperature-dependent behaviour of PV modules. The chosen parameter to be analysed has been the Ross coefficient, a critical parameter for characterizing module performance under varying temperatures, that has been determined through a graphical approach by plotting irradiance against the temperature difference between each module and ambient air. In the

Table 3

Standard deviation for the measured open circuit voltage (Voc) and fill factor (FF), broken by modules size.

| | 12 cells | 24 cells | 6 cells |
|----------------|----------|----------|---------|
| σ (Voc) | 0.059 | 0.110 | 0.025 |
| σ (FF) | 0.677 | 0.437 | 0.489 |

following paragraphs, the calculation of the Ross coefficient is provided, and the preparation of the data set is described, which allowed to clean the data from statistical and systematic measurement errors.

3.2.1. Data cleaning

To ensure data quality and remove outliers, a code written in Python 3.9.7 was employed to access and process the data. For the temperature related behaviour, to ensure the consideration of clear sky conditions, filtering procedures, as reported in [7], were implemented. Data points corresponding to a ratio of diffuse and global irradiance greater than 0.20 were excluded, as direct irradiance was found to be the predominant component under such conditions. A subsequent phase of analysis was carried out with the application of specific additional filters. The first filter selects only values corresponding to an irradiance level higher than 300 W/m², since the inspection on the raw data showed a good quality of the measurements in that range. A second filter selected only the values within the range of $PR_{avg} \pm 2\sigma$, where PR_{avg} represented the average value of the performance ratio of the PV array for the specified period, as defined by the international standard IEC 61724 [8]. The

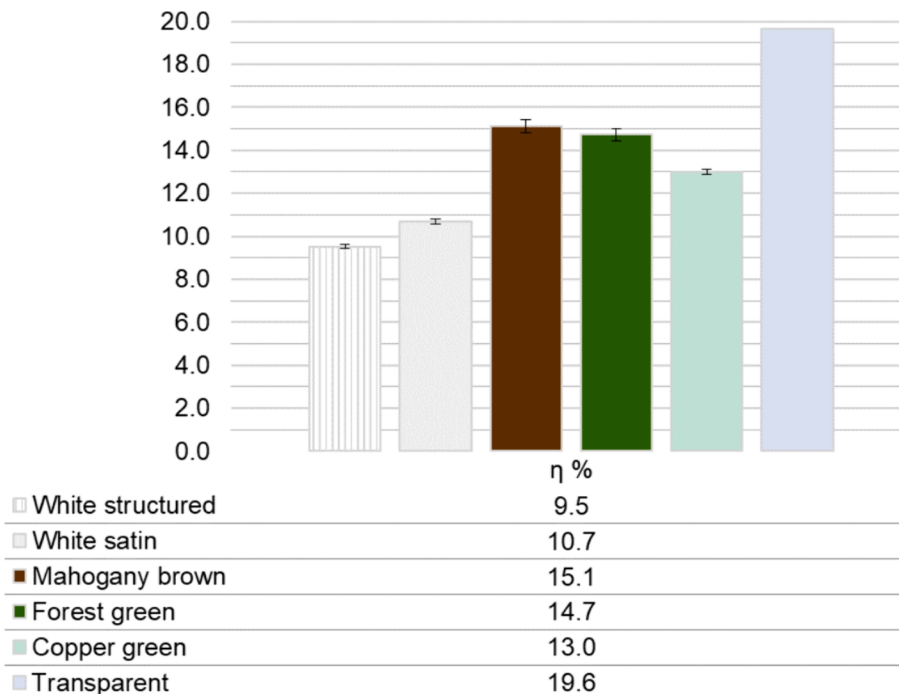


Fig. 11. Coloured modules average efficiencies, broken by colour, compared to a reference transparent module.

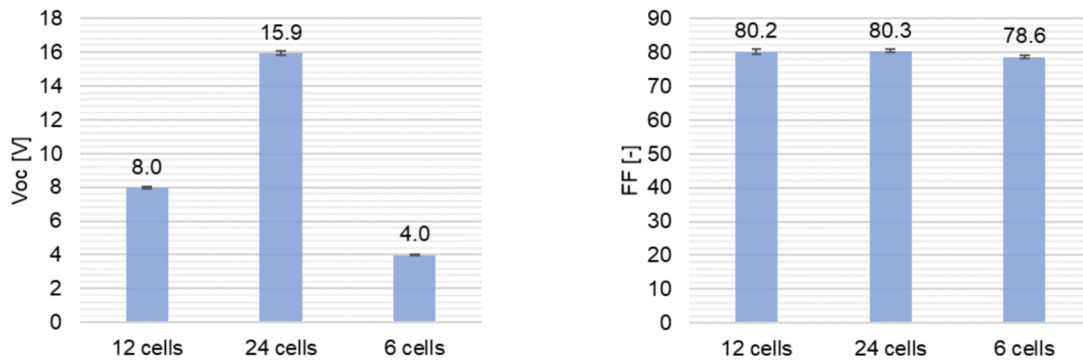


Fig. 12. Indoor test results on modules of different sizes (including all colours): variance associated to the open circuit voltage (Voc) and fill factor (FF).

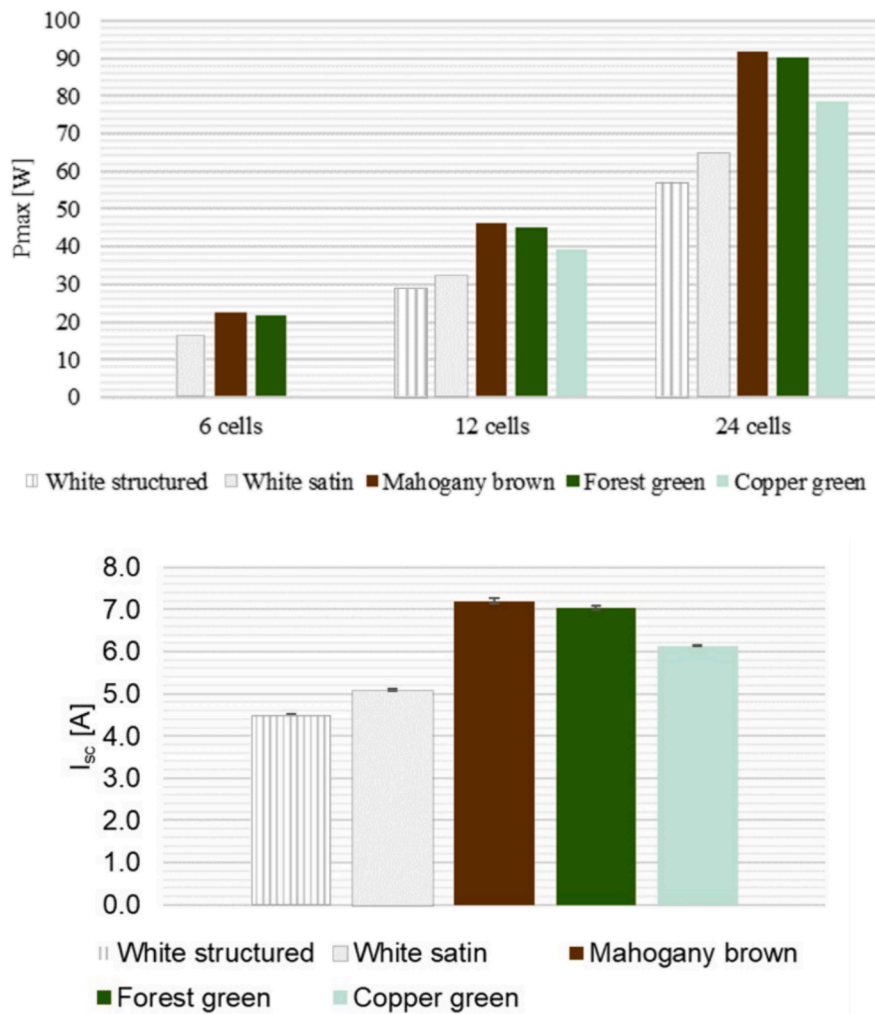


Fig. 13. Indoor test results on modules of different sizes: maximum power (Pmax) and short circuit current (Isc).

performance ratio (PR) was computed based on the formula (EQ. 2):

$$PR = \frac{E \cdot \hat{A} \cdot G_{STC}}{P_n \cdot \hat{A} \cdot G} \quad (2)$$

where E denoted the instant power produced (W), Pn was the array nominal power (W), G_{STC} represented the irradiance under STC conditions (1000 W/m²), and G was the instant irradiance (W/m²). The standard deviation (σ) was utilized to establish the permissible range for data inclusion. To remove the dependency of I_{MPP} and P_{MPP} on

irradiance, the data were translated to an STC irradiance of 1000 W/m². Subsequently, a linear regression model from the scipy.stats module in Python was utilized to conduct a linear regression over the data. Outliers were identified as data points exceeding the standard deviation in normalised I_{MPP}, as I_{MPP} and P_{MPP} tended to exhibit a higher occurrence of outliers, necessitating a more rigorous threshold for data cleaning. The last two filters allowed to clean the dataset from fault measurements due to differential shading occurred between the modules and the POA (plan of array) pyranometer. These robust data cleaning procedures facilitated

a thorough and reliable analysis of the temperature-dependent behaviour of the PV modules, described in detail in the following sections. For the energy yield analysis reported in section 3.5.4, a simple filter excluding nighttime has been applied.

3.2.2. Outdoor monitoring results: Ross coefficient

The Ross model is a widely used temperature model in the PV sector. It assumes a linear relationship between the temperature difference of the PV module and the ambient temperature ($T_m - T_a$) and the

irradiance on the plane of array (G_{POA}) (EQ. 3). The constant k, which varies with different boundary conditions, is specific to the module's design and materials [9].

$$T_m = T_a + k \cdot G_{POA} \tag{3}$$

The Ross coefficient for the analysed modules has been determined through a graphical approach by plotting irradiance against the temperature difference between each module and ambient air. An intercept was thus identified among the scattered data points implementing the

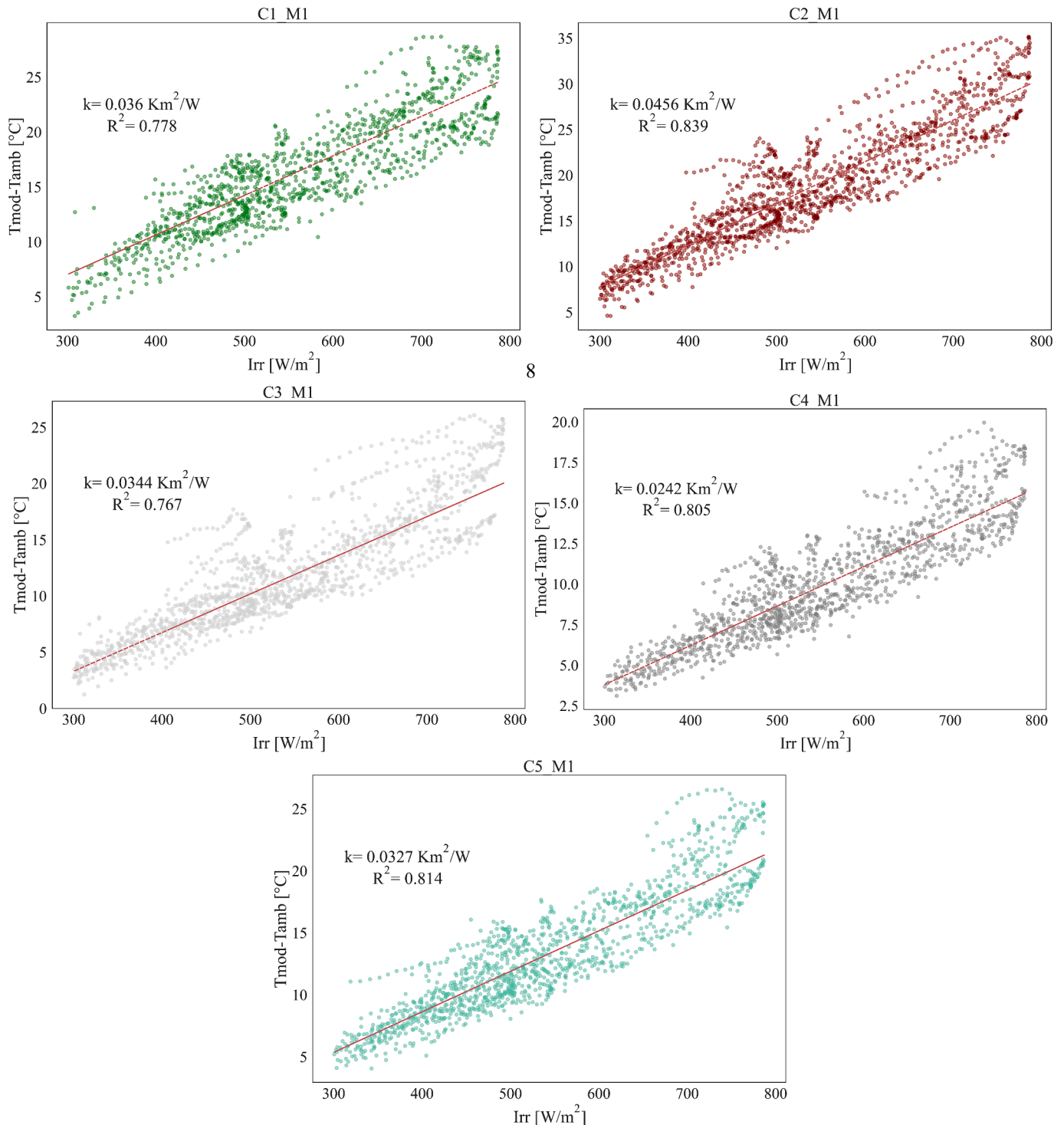


Fig. 14. Example of graphic identification of the Ross coefficient for 24 cells modules (M1) for the five analysed colours. The slope of the intercept of the scattered datapoints represents the Ross coefficient.

Theil Sen regression method via the Python’s scipy.stats package. The slope of the resulting line represents the value of the Ross coefficient. In Fig. 14 examples of the intercept and the scatter data points are reported for the 24 cells modules (M1) for each analysed colour. In Fig. 15 and Table 4 the Ross coefficients for each analysed module are reported. Higher Ross coefficients indicate a higher module’s operating temperature, which are usually due to poor module’s back ventilation rate, as reported in the literature [10,11]. Typical values of Ross coefficient for specific mounting strategy are reported in Table 5. The Ross coefficients measured for the analysed modules are consistent with the values found in the literature for not so well cooled applications, such as flat roof and façade integrated semi-transparent PV [11,12].

All the analysed modules seem to perform better than literature reported opaque façade integrated PV modules, which typically present a Ross coefficient over 0.05 K m²/W (Table 5, [10,11]). By analysing the results, the modules’ colour seems to introduce an additional variability factor for the modules’ temperature dependent behaviour. Indeed, the mahogany brown modules, which have shown the highest power output and efficiency after indoor testing, highlight a higher Ross coefficient, followed (in average) by the forest green, the copper green and the withes. The higher power output at standard test condition can be explained by the higher absorption of photons of the active layer, due to a high degree of transparency of the coloured glass over the spectral response range of the analysed active technology, which include a portion of the infrared spectrum, until 1100 nm. Indeed, several studies found in the literature [12,13,14] reported that, usually, to reproduce modules which display darker colours, a smaller number of coloured dyes are required to produce the coloured filter, if compared to brighter colours. As a result, a dark colour filter presents a higher spectral transmittance, allowing a higher portion of the radiation on the electromagnetic spectrum to reach the PV cells beneath, producing more power. The higher rate of absorbed irradiance at the active surface provokes a higher operating temperature for the module which, being the ambient parameters held constant, results in a higher Ross coefficient. In addition, the light absorption in the coloured layer can contribute to a further increase in the system’s temperature, as demonstrated by Babin et al. in [15]. Variability of the Ross coefficient among modules of the same colour, might be due to slightly different local back ventilation conditions. Indeed, the ventilation in the air gap between the BIPV cladding and the wooden substructure might be influenced by the activation of a chimney effect due to a temperature gradient along the façade height, which is of 4 m. Besides, local turbulence in the air gap might be caused by the temperature sensors cabling, which run in the cavity. To deepen the understanding of this effect, a

Table 4
Values of the calculated Ross coefficients (k) for the monitored modules.

| | C1 – Forest green | C2 – Mahogany brown | C3 – White satin | C4 – White structured | C5 – Copper green |
|----|-------------------|---------------------|------------------|-----------------------|-------------------|
| M1 | 0.036 | 0.0456 | 0.0344 | 0.0242 | 0.0327 |
| M2 | 0.0295 | 0.0406 | 0.0332 | 0.0294 | 0.0311 |
| M3 | 0.033 | 0.0414 | 0.032 | 0.0302 | 0.0334 |
| M4 | 0.028 | 0.04 | 0.0311 | 0.0342 | |
| M5 | 0.035 | 0.0381 | 0.029 | | |
| M6 | | | 0.0279 | | |

Table 5
Ross coefficient (k) values found in the literature [10,11].

| PV Array Mounting Type, Module Type | k (K m ² /W) |
|--|-------------------------|
| Free-standing | 0.021 |
| Flat roof | 0.026 |
| Sloped roof, well-cooled | 0.020 |
| Sloped roof, not-so-well cooled | 0.034 |
| Sloped roof, highly integrated and poorly ventilated | 0.056 |
| Façade-integrated, semitransparent PV | 0.046 |
| Façade-integrated with narrow gap, opaque PV | 0.054 |

statistical analysis of the temperatures on the BIPV modules’ back surfaces is provided in the next section.

3.2.3. Modules’ back surface temperature distribution

As the previous section highlighted, back ventilation is a crucial aspect to be evaluated for the behaviour of BIPV installations. In the air gap between the cladding and the wooden substructure, temperature gradient might induce a chimney effect, thus providing a certain improved degree of ventilation for the modules. As a first evaluation of a potential induced chimney effect in the cavity module’s temperatures statistical distribution during the operation periods (i.e. excluding nighttime and periods of predominant diffuse irradiance, see section 3.5.1) have been plotted. The plots in Fig. 16 show the statistical distribution of the back temperatures for one module of each colour in each row of the mock-up. From the data one can notice that the modules follow the expected behaviour from the Ross coefficient, with the darker modules in each row presenting the higher temperatures.

To investigate the activation of the back ventilation induced by a temperature gradient, the difference in temperature between the highest and the lowest temperature sensors for each column has been plotted. In Fig. 17 the columns have been identified by the relative colour of the

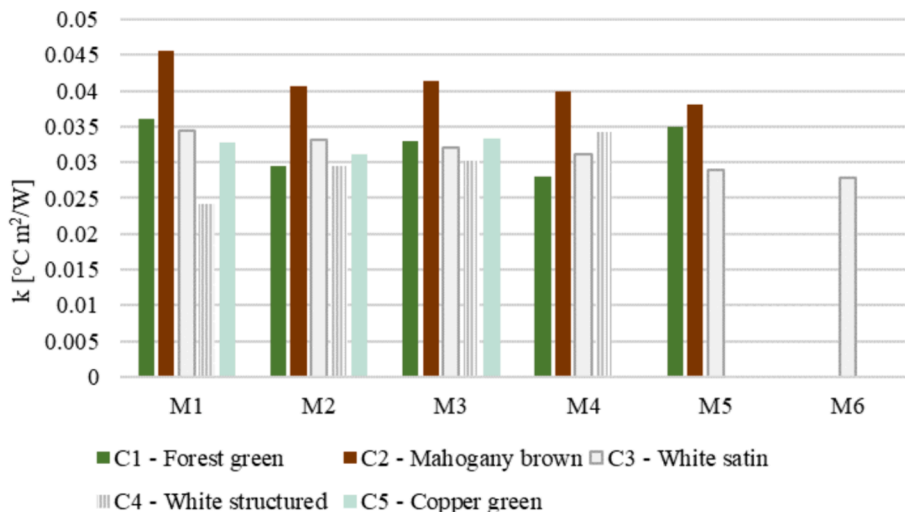


Fig. 15. Calculated Ross coefficients (k) for the monitored modules.

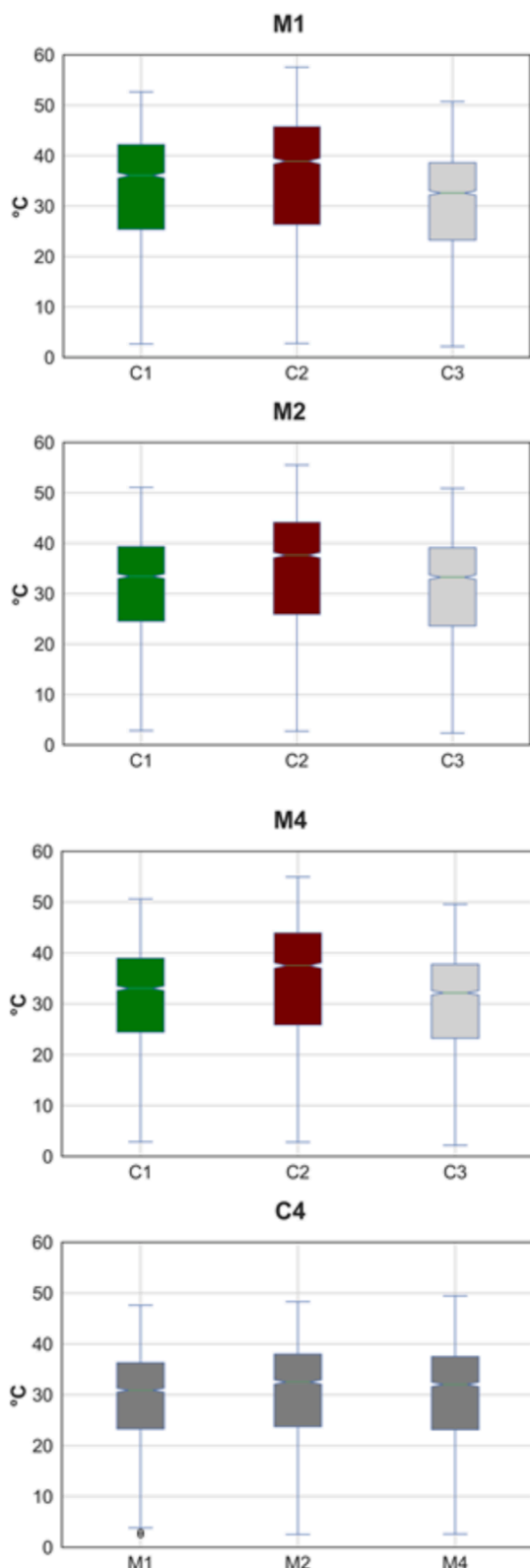


Fig. 16. Statistical distribution of the back temperatures for one module of each colour. from the top: row (M1), row (M2), and row (M4) and row(C4). Each box shows the interquartile range of the dataset for each colour, with the lower and upper edges of the box representing the first (Q1) and third quartiles (Q3), respectively. The box shrinking inside the box indicates the dataset median. The “whiskers” extend from the box to the smallest and largest values within 1.5 times the interquartile range from Q1 and Q3, respectively. Dataset outliers and are plotted as individual points.

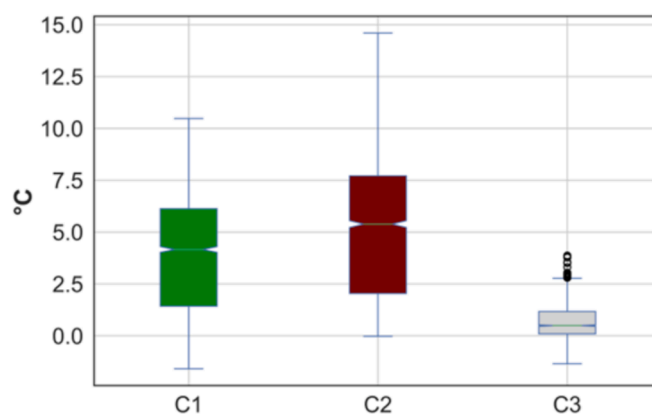


Fig. 17. Difference in temperature between the highest and the lowest temperature sensors for each colour. Each box shows the interquartile range of the dataset for each colour, with the lower and upper edges of the box representing the first (Q1) and third quartiles (Q3), respectively. The box shrinking inside the box indicates the dataset median. The “whiskers” extend from the box to the smallest and largest values within 1.5 times the interquartile range from Q1 and Q3, respectively. Dataset outliers and are plotted as individual points.

upper part of the installation. It is interesting to notice that the darker colour (C2, mahogany brown) presents an average temperature gradient of more than 5 °C, while the green has a difference of about 4,5 °C, and the white column of less than 1 °C. These results might indicate that darker colour induces stronger temperature gradient in the air gap behind the rainscreen façade, due to the stronger temperature induced behaviour described in section 3.5.2 by the Ross coefficient.

To deepen this topic, the temperature observations should be analyzed together with the measured air velocity in the air cavity. Indeed, anemometers were installed in the mock-up cavity, but the acquired measurements were affected by local turbulences caused by the presence of temperature sensor cabling running through the cavity. Therefore, such a combined analysis has not been possible with the available data.

3.2.4. Energy yield

The effect of varying temperature-related behavior for different colors can be appreciated by analyzing the energy yield. The yield has been calculated by integrating the power output recorded by the microinverter during the module string operation and dividing the obtained energy by the active surface area of each string. From Fig. 18 one can highlight that the difference in efficiency between C1 and C2 (−2.7 %) measured during indoor testing translate in a lower difference concerning the outdoor energy yield (−0.3 %). This might be due to the beneficial effect of the green glass, that probably has slightly higher reflectance, both in the visible and in the infrared region of the electromagnetic spectrum, than the mahogany one, resulting in a lower Ross coefficient and thus a lower operating temperature observed through the data analysis. The same is observed for C3 (satin white), which has an efficiency lower than 29.4 % compared to the mahogany (C2), while the outdoor energy yield results to be lower only by −14.7 %, and the copper green, which compared to the mahogany has an efficiency lower that 14.1 %, while the yield is lower that 4.6 %. The structured white also presents a decrease in difference between the relative percentual efficiency and yield, but of lower intensity. This might be related to the three-dimensional glass structure, which could cause a higher optical path for the light and a different incidence angle modifier (IAM) for these samples. It is necessary to highlight that slight difference in the yield might be due to the efficiency of the installed connections systems and cabling, which are separated for each colour string.

These results are of crucial importance for the research in the field of coloured BIPV, firstly because data of such a kind are extremely scarce in the literature, and secondly because they offer very good information for

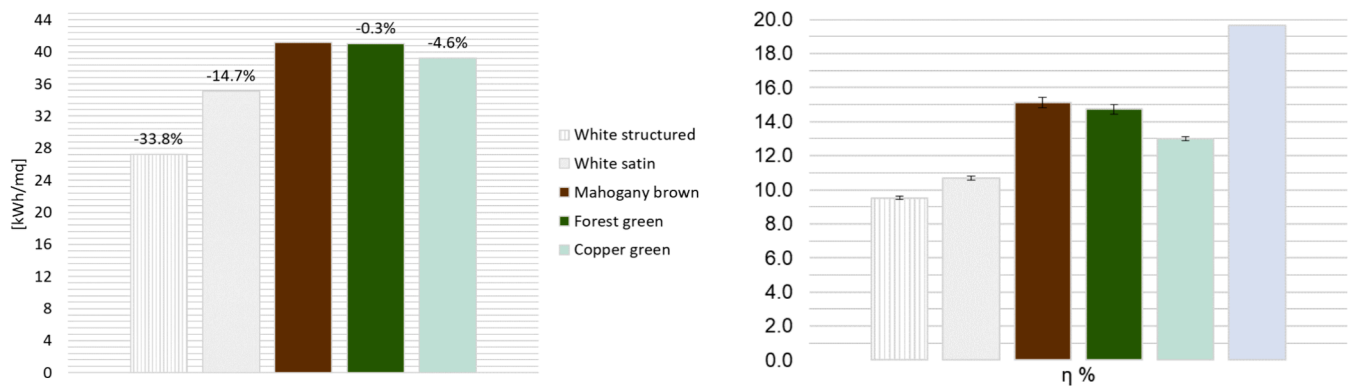


Fig. 18. Energy yield per square meter (on the left), during the analysed period, for the different coloured BIPV strings. On the right, the efficiency calculated at STC have been reported to allow direct comparison with the yield.

the optimization of the product characteristics and production.

4. Conclusion

The outcomes of this research underscore a pivotal advancement in understanding the dynamics governing the performance of coloured customized PV modules. The INFINITE project's real-scale mock-up within the PV Integration Lab of Eurac Research, has served as an essential platform for unraveling the relationship between aesthetic features and energy efficiency in colored PV modules.

In particular, the extensive monitoring campaign undertaken in this study has unearthed critical mechanisms influencing the performance of coloured BIPV modules under real operating conditions. Unlike indoor tests alone, which may overlook key environmental factors, this research has delved into the nuanced interplay of variables that impact BIPV module performance in real-world settings.

By investigating the performance of BIPV modules across five colours and finishing types, both indoors and in operating exposure conditions, this work has shed light on real exposure behavior of coloured BIPV technology. The study highlights new mechanisms that emerge during operational phases, particularly regarding temperature dynamics associated with different colors.

By analyzing the energy yield of the monitored modules, the data show how different colors behave at varying temperatures. Indeed, the efficiency difference between colors indoors doesn't always match outdoor energy yield.

The results suggest that this might be because of the coloured layer, which determine a different temperature related behavior of the modules.

In particular, the mahogany brown modules, which have shown the highest power output and efficiency after indoor testing, highlight a higher Ross coefficient (with the measured highest Ross coefficient = $0.0456 \text{ K m}^2/\text{W}$), followed (in average) by the forest green, the copper green and the withes (with the measured lowest Ross coefficient = $0.0242 \text{ K m}^2/\text{W}$).

The impact of Ross coefficient variations across different colors influences the final energy yield, counteracting the STC (standard test condition) efficiency values of these colors. Darker colors exhibit higher STC efficiency and thus tend to have a greater energy yield. However, they also display the highest Ross coefficient values, resulting in a more pronounced decrease in performance due to temperature increases. Conversely, lighter colors, despite having a lower energy yield due to reduced efficiency under Standard Test Conditions (STC), exhibit lower Ross coefficient values and consequently experience less performance degradation from temperature effects.

These findings are crucial for colored BIPV research because similar data are hard to find. Plus, they help to improve product design and production methods. The discovery of these underlying mechanisms

paves the way for more informed decision-making processes among designers, architects, and policymakers, facilitating the development of more effective and sustainable building practices. The findings of this study represent a significant step forward in bridging the gap between aesthetic considerations and energy performance in BIPV installations, highlighting the critical importance of conducting research in real operating conditions to fully comprehend the complexities of PV customized technologies integrated in the built environment.

CRediT authorship contribution statement

Martina Pelle: Writing – review & editing, Writing – original draft, Visualization, Validation, Software, Methodology, Investigation, Formal analysis, Data curation, Conceptualization. **Martino Gubert:** Writing – original draft, Supervision, Resources, Project administration, Funding acquisition, Conceptualization. **Enrico Dalla Maria:** Writing – review & editing, Software, Resources, Data curation. **Alexander Astigarraga:** Writing – review & editing. **Stefano Avesani:** Project administration, Funding acquisition. **Laura Maturi:** Writing – review & editing, Writing – original draft, Supervision, Methodology, Conceptualization.

Declaration of competing interest

The authors declare that they have no known competing financial interests or personal relationships that could have appeared to influence the work reported in this paper.

Data availability

Data will be made available on request.

Acknowledgement

The INFINITE project has received funding from the European Union's Horizon 2020 research and innovation programme under grant agreement No 958397. This paper reflects only the author's view, neither the European Commission nor HADEA are responsible for any use that may be made of the information it contains.

This study was developed in the framework of the research activities carried out within the Project "Network 4 Energy Sustainable Transition—NEST", Spoke 1., Project code PE0000021, funded under the National Recovery and Resilience Plan (NRRP), Mission 4, Component 2, Investment 1.3— Call for tender No. 1561 of 11.10.2022 of Ministero dell'Università e della Ricerca (MUR); funded by the European Union - NextGenerationEU. *Investimento 1.3 - Avviso "Partenariati estesi alle università, ai centri di ricerca, alle aziende per il finanziamento di progetti di ricerca di base.*

The authors would like to thank the companies SUNAGE and

RUBNER Holzbau for the mock-up manufacturing. The authors would like to thank Lukas Koester, Alexander Astigarraga, Stefano Donzelli and Valentino Diener for the mock-up construction and their contribution to the indoor and outdoor tests.

References

- [1] European Commission, "Clean Energy For All Europeans. Clean Energy For All Europeans. European Commission." Accessed: Apr. 05, 2020. [Online]. Available: https://ec.europa.eu/energy/topics/energy-strategy/clean-energy-all-europeans_en.
- [2] European Parliament, *DIRECTIVE (EU) 2018/844. Energy performance of buildings*. 2018.
- [3] S. Michas, V. Stavrakas, N.-A. Spyridaki, A. Flamos, Identifying research priorities for the further development and deployment of solar photovoltaics, *Internat. J. Sustain. Energy* 38 (3) (2019) 276–296, <https://doi.org/10.1080/14786451.2018.1495207>.
- [4] L. Maturi, J. Adami, *Building Integrated Photovoltaic (BIPV) in Trentino Alto Adige. Green Energy and Technology.*, Springer International Publishing, Cham, 2018 doi: 10.1007/978-3-319-74116-1.
- [5] M. Pelle, E. Lucchi, L. Maturi, A. Astigarraga, F. Causone, Coloured BIPV technologies: methodological and experimental assessment for architecturally sensitive areas, *Energies (Basel)* 13 (17) (2020) 4506, <https://doi.org/10.3390/en13174506>.
- [6] R. Roverso, et al., *Experimental assessment and data analysis of colored photovoltaic in the field of BIPV technology application*. 38th European Photovoltaic Solar Energy Conference and Exhibition, 2021.
- [7] L. Maturi, G. Belluardo, D. Moser, M. Del, BiPV system performance and efficiency drops: overview on PV module temperature conditions of different module types, *Energy Procedia* 48 (2014) 1311–1319, <https://doi.org/10.1016/j.egypro.2014.02.148>.
- [8] International Electrotechnical Commission, "IEC 61724-1:2021 - Photovoltaic system performance - Part 1: Monitoring," 2021.
- [9] R.G. Ross, Interface design considerations for terrestrial solar cell modules, in: *Proceedings of the IEEE Photovoltaic Specialists Conference, Baton Rouge, La, 1976*, pp. 801–806.
- [10] T. Nordmann, L. Clavadetscher, Understanding temperature effects on PV system performance, in: *Proceedings of 3rd World Conference on Photovoltaic Energy Conversion, Osaka, 2003*, pp. 2243–2246.
- [11] N. Martín-Chivelet, J. Polo, C. Sanz-Saiz, L.T. Núñez Benítez, M. Alonso-Abella, J. Cuenca, Assessment of PV module temperature models for building-integrated photovoltaics (BIPV), *Sustainability* 14 (3) (2022) 1500, <https://doi.org/10.3390/su14031500>.
- [12] M. Pelle, F. Causone, L. Maturi, D. Moser, Opaque coloured building integrated photovoltaic (BIPV): A review of models and simulation frameworks for performance optimisation, *Energies (Basel)* 16 (4) (2023) 1991, <https://doi.org/10.3390/en16041991>.
- [13] M. Pelle, E. Canosci, G. Luzzi, L. Maturi, Hidden colored Building Integrated Photovoltaics: technology overview and design challenges. *International Conference on Solar Energy for Buildings and Industry, Kessel, 2022*.
- [14] A. Røyset, T. Kolås, B.P. Jelle, Coloured building integrated photovoltaics: Influence on energy efficiency, *Energy Build* 208 (2020), <https://doi.org/10.1016/j.enbuild.2019.109623>.
- [15] M. Babin, I.H. Jóhannsson, M.L. Jakobsen, S. Thorsteinsson, Experimental evaluation of the impact of pigment-based colored interlayers on the temperature of BIPV modules, *EPJ Photovoltaics* 14 (2023) 34, <https://doi.org/10.1051/epjpv/2023028>.